Volume 17 | Number 3 | 7 February 2017 | Pages 353–570

Lab on a Chip

Miniaturisation for chemistry, physics, biology, materials science and bioengineering

rsc.li/loc

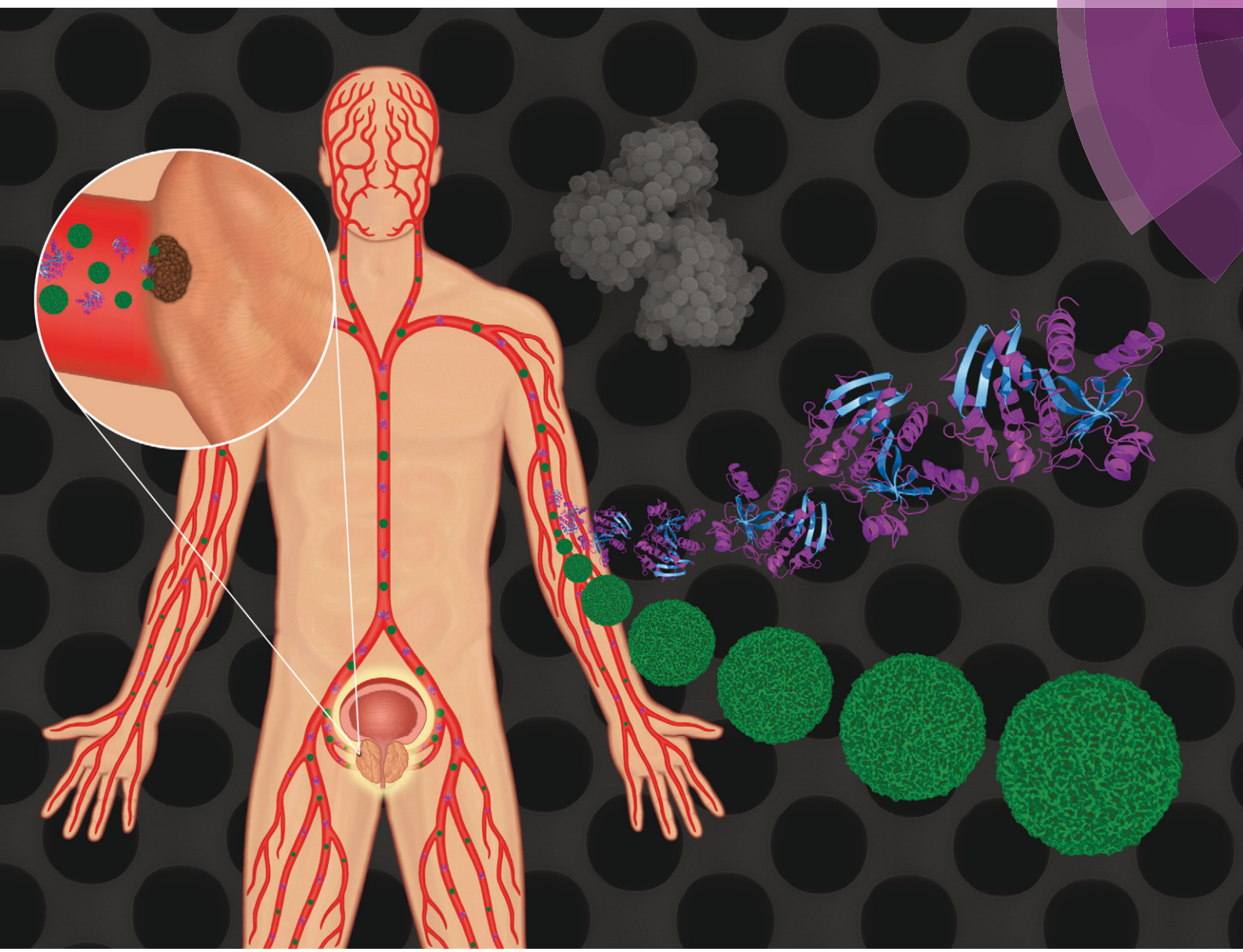

ISSN 1473-0197

ROYAL SOCIETY OF CHEMISTRY

PAPER

Cagri A. Savran *et al.*

Separation and dual detection of prostate cancer cells and protein biomarkers using a microchip device

Lab on a Chip

PAPER

View Article Online
View Journal | View Issue

Cite this: *Lab Chip*, 2017, **17**, 415

Separation and dual detection of prostate cancer cells and protein biomarkers using a microchip device†

Wanfeng Huang,[ab] Chun-Li Chang,[ab] Norman D. Brault,[ab] Onur Gur,[ab] Zhe Wang,[ab] Shadia I. Jalal,[d] Philip S. Low,[e] Timothy L. Ratliff,[f] Roberto Pili[gh] and Cagri A. Savran*[abc]

Current efforts for the detection of prostate cancer using only prostate specific antigen are not ideal and indicate a need to develop new assays – using multiple targets – that can more accurately stratify disease states. We previously introduced a device capable of the concurrent detection of cellular and molecular markers from a single sample fluid. Here, an improved design, which achieves affinity as well as size-based separation of captured targets using antibody-conjugated magnetic beads and a silicon chip containing micro-apertures, is presented. Upon injection of the sample, the integration of magnetic attraction with the micro-aperture chip permits larger cell–bead complexes to be isolated in an upper chamber with the smaller protein–bead complexes and remaining beads passing through the micro-apertures into the lower chamber. This enhances captured cell purity for on chip quantification, allows the separate retrieval of captured cells and proteins for downstream analysis, and enables higher bead concentrations for improved multiplexed ligand targeting. Using LNCaP cells and prostate specific membrane antigen (PSMA) to model prostate cancer, the device was able to detect 34 pM of spiked PSMA and achieve a cell capture efficiency of 93% from culture media. LNCaP cells and PSMA were then spiked into diluted healthy human blood to mimic a cancer patient. The device enabled the detection of spiked PSMA (relative to endogenous PSMA) while recovering 85–90% of LNCaP cells which illustrated the potential of new assays for the diagnosis of prostate cancer.

Received 15th October 2016,
Accepted 9th December 2016

DOI: 10.1039/c6lc01279e

www.rsc.org/loc

Introduction

Prostate cancer is the most commonly occurring cancer for men in the United States. In 2016 alone, the estimated numbers of newly diagnosed cases and deaths associated with prostate cancer are 180 890 and 26 120, respectively.[1] In an effort to reduce the impact of prostate cancer on society, there has been a major push towards early detection strategies to help stop the disease before it becomes life threatening. Critical to this effort is the discovery and validation of biomarkers (*e.g.* proteins, DNA, metabolites, cells, *etc.*) which is of great significance not only because these analytes are important for early diagnostic screening tests, but also due to their roles in establishing prognosis and monitoring response to therapy, among other uses.[2–10] While multiple biomarkers have been investigated for the detection of prostate cancer, including prostate specific membrane antigen (PSMA), micro-RNA, and survivin, the most commonly used biomarker for diagnosing prostate cancer is the protein, prostate specific antigen (PSA).[11–13] PSA is detectable *via* a number of available and highly sensitive assays.[14] However, the extensive use of diagnostic screening tests based primarily on PSA are controversial, so much so, that in 2012 the United States Preventive Task Force concluded that the risks of such routine blood tests (*e.g.* unneeded surgery and radiation) outweighed the benefits of early detection and thus recommended reduced testing.[15] This has led to the search for additional biomarker candidates that can better stratify different disease states.

One type of target that has been extensively studied and validated for use in prostate cancer is circulating tumor cells

[a] *School of Mechanical Engineering, Purdue University, West Lafayette, IN, 47907, USA. E-mail: savran@purdue.edu*
[b] *Birck Nanotechnology Center, Purdue University, West Lafayette, IN, 47907, USA*
[c] *Weldon School of Biomedical Engineering, Purdue University, West Lafayette, IN, 47907, USA*
[d] *Department of Medicine, Indiana University School of Medicine, Indianapolis, IN, 46202, USA*
[e] *Department of Chemistry, Purdue University, West Lafayette, IN, 47907, USA*
[f] *Center for Cancer Research and Department of Comparative Pathobiology, Purdue University, West Lafayette, IN, 47907, USA*
[g] *Genitourinary Program, Roswell Park Cancer Institute, Buffalo, NY, 14263, USA*
[h] *Genitourinary Program, Indiana University-Simon Cancer Center, Indianapolis, IN, 46202, USA*

† Electronic supplementary information (ESI) available. See DOI: 10.1039/c6lc01279e

(CTCs).[16,17] CTC biomarkers are commonly isolated *via* immuno-magnetic bead-based separation assays by targeting specific cell-surface markers such as epithelial cell-adhesion molecule (EpCAM), cytokeratin, PSMA, vimentin, and others.[18–21] Prostate CTCs have recently been found to be correlated with a number of other recognized targets (*e.g.* lactate dehydrogenase, alkaline phosphatase, PSA) and used in combination for treatment monitoring and survival prediction of prostate cancer patients.[22,23] For example, the use of the CellSearch platform for CTC detection combined with a real-time quantitative polymerase chain reaction (qPCR) assay enabled an approach consisting of CTC enumeration and stem cell gene expression analysis to be applied and used to determine the prognosis and predict treatment outcomes in a metastatic castration-resistant prostate cancer model.[24] This example demonstrates the need and advantage of developing biomarker panels *via* multiplexed target analysis.

However, the widespread implementation of such multiplex analysis requires overcoming several barriers and limitations.[2,3,25–27] These include inter-individual variability, reliability, sensitivity and specificity during analyte detection, all of which have led to significant measurement deviations.[28] Additionally, multiple biomarker platforms are often employed to perform numerous individual tests, often at great expense, in order to provide sufficient reliable information for patient evaluation.[19,29–31] This has led to the need for high-throughput detection platforms capable of analysing multiple biomarkers simultaneously from a single sample.

Several commercial high-throughput platforms for multiplexed protein analysis are widely available (*e.g.* Luminex, MSD) and academic groups along with industry are actively pursuing methods for the detection and analysis of cancer cells (*e.g.* CTCs) from large sample volumes. However, it is not ideal to measure proteins *or* cells, separately, which is the case with most biosensor platforms.[8,32–38] As the CTC capture and stem cell gene expression study above illustrated, valuable information can be gathered from both cellular and molecular biomarkers. Additionally, by more accurately correlating molecular biomarker concentrations in a sample fluid with specific cell populations present, which would be possible with a dual-detection platform, new biomarker panels could be developed to better describe a patient's disease state and provide a more holistic analysis.[39] Analysing a single sample for multiple target types – cells and molecules – should also lead to reduced sample-to-sample variation.[40–42]

We previously introduced a device capable of the concurrent detection of cellular and molecular markers, in high throughput, from a single sample fluid. This device utilized a glass slide integrated with a magnet for attracting cellular and molecular biomarkers bound to antibody-conjugated magnetic beads.[43] While this preliminary system successfully demonstrated the ability to simultaneously detect cellular and molecular targets from an ovarian cancer patient sample (ascites fluid), several limitations were observed. These include captured cells being buried under bead clusters (see ESI† Fig. S1), which was exacerbated when higher bead concentrations were used. The clusters of beads on top of cells reduced the cell purity (especially for fluorescence imaging purposes) and the combination of captured cells and molecular markers, with any remaining beads, all on the same surface also reduced the ability to retrieve the cells for downstream analysis (*e.g.* genetic sequencing, culturing, *etc.*). As the concentration of CTCs in patient samples are very low, the inability to increase the bead amount conversely affected the ability for multiplexed ligand targeting, which could be used for not only capturing additional protein/molecular analytes but also for increasing the number of CTCs detected.

In this study, we have developed a next generation system that combines rapid fluid flow with size-based separation to realize a high-throughput immuno-magnetic detection platform for the simultaneous separation and detection of molecular and cellular targets. The new version divides magnetically captured cellular and molecular targets into upper and lower chambers, respectively, *via* the use of a silicon chip containing 6 μm diameter micro-aperture holes. Upon incubating a liquid sample with antibody-conjugated magnetic beads targeting desired cells and protein biomarkers, the sample is then flowed through the upper chamber of the device. The integration of an external magnetic force with the micro-aperture chip allows the larger cell-bead complexes (>8 μm) to be trapped on top of the chip, with the smaller protein-bead complexes (1 μm) and remaining beads passing through the micro-aperture holes into the lower chamber where the magnetic force holds them in place on a bottom surface.

There are multiple advantages of the new generation device. First, due to the efficient elimination of non-cell complexed beads from the upper chamber, both captured cells and molecules can be analysed separately without mutual interference.[32] The cells can be quantified directly on chip and then removed for further investigation. Protein-bound beads can be retrieved from the bottom chamber and analysed using fluorescence-based detection or with other commercially available assays. Lastly, this design enables the use of higher bead concentrations.

Materials and methods

In this study, we characterized the new device in the context of a prostate cancer model by dual detection of the free PSMA protein and LNCaP cells, using the two antibodies, anti-PSMA and anti-EpCAM.[44,45] EpCAM and PSMA cell surface markers have been previously used to isolate prostate cancer CTCs.[46] The LNCaP cell line is a commonly applied model for prostate cancer and has been shown to express both EpCAM and PSMA antigens on the cell surface, making it particularly relevant to our work.[47–49] As EpCAM is one of the most commonly used markers for capturing CTCs in breast, colon, and prostate cancers, its use with LNCaP cells also enables the device characterization to be more generalized to other diseases.[50] The cell-free PSMA protein was chosen due

to its value, from an analytical perspective, to challenge the new device by using a free protein target that is also on the surface of the cell, in combination with a ligand (EpCAM) specifically targeting only the cell itself. This contrasts with the scenario in which the free protein and cells would be captured using completely different antibodies. While the presence of free PSMA protein in circulation has been studied, the clinical significance of detecting PSMA alone for prostate cancer remains uncertain.[51,52] Thus, a method to simultaneously detect the free PSMA protein as well as prostate cancer cells might allow for the discovery of new diagnostic value for PSMA.

This paper first presents the overall detection strategy, device assembly and operation, followed by numerical modeling. Next, multiple ligands conjugated to magnetic beads are investigated to achieve maximal cell capture yield. Using culture media, the limit of detection for PSMA as well as the performance in dual analyte capture is then determined. Finally, the potential of the device for clinical application is demonstrated using diluted human blood spiked with PSMA and LNCaP cell targets, to mimic prostate CTCs and protein biomarkers from a patient sample.

Detection strategy

The detection strategy is illustrated in Fig. 1. Superparamagnetic streptavidin coated microparticles are first conjugated to their corresponding biotinylated polyclonal antibodies. A sample fluid containing spiked LNCaP cells and PSMA protein (Fig. 1a) is then combined with the antibody conjugated-bead (anti-bead) mixture and incubated for 90 min using an end-over-end rotator.

The microfluidic device is divided into two parallel chambers separated by a micro-aperture chip composed of an array of 6 μm diameter micro-apertures (2.6×10^5 holes in total). Following sample incubation, the mixture is flowed through the upper chamber (Fig. 1b) at a flow rate of 2 mL min^{-1} and circulated for 4 min. A permanent magnet

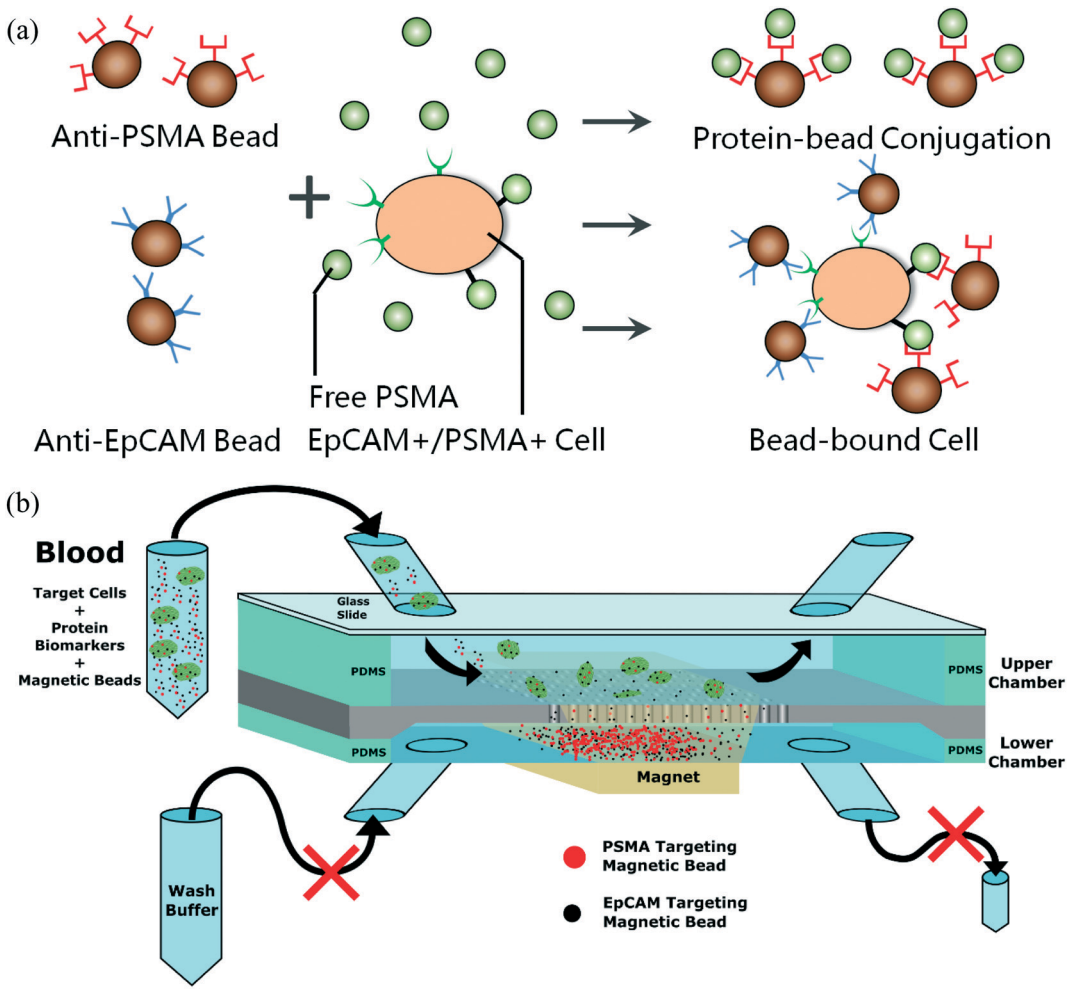

Fig. 1 Schematic diagram of the detection strategy. (a) Rare cells and proteins are simultaneously captured by streptavidin-coated magnetic beads conjugated with antibodies. (b) Sample is flowed through the upper chamber of the device in which captured cells and proteins are size-separated *via* the micro-aperture chip. Protein-bound and free beads in the lower chamber can be removed by stopping flow in the upper chamber, removing the magnet, and washing the lower chamber with buffer. The collected sample containing magnetic beads can be analysed off-chip using fluorescence analysis for protein quantification. Cells can be directly quantified on-chip.

positioned beneath the device provides the magnetic field to pull the bead-bound cells and proteins, as well as free beads, towards the micro-aperture chip. The protein-bead complexes and free beads, owing to their smaller size (1 μm), can be drawn down to the lower chamber through the micro-apertures whereas cell-bead complexes, due to their larger size (>8 μm), are retained on top of the micro-aperture chip in the upper chamber. The cell and molecular targets, in the upper and lower chambers, respectively, are then subjected to separate fluorescence-based quantitative assays. The cells are enumerated on the chip surface. The protein-bound beads are retrieved from the lower chamber by introducing washing buffer with the magnet removed and then analysed *via* fluorescence microscopy.

An important advantage of this strategy is that it does not require the centrifugation of the original sample during the detection of target analytes. For example, common methods for cell capture first involve the centrifugation of a blood sample (to fractionate target cells) and the subsequent aspiration (removal) of the appropriate liquid layer. However, a major disadvantage to this process is that it can lead to significant user-to-user error while compounding the risk of losing rare cells such as CTCs. As all steps associated with the detection strategy in this work are additive, the new device and the assay demonstrated avoid the downfalls associated with methods of cell capture that involve centrifugation.

System and device assembly

The microfluidic device consists of eight components: an acrylic cover, acrylic stand, top fluid cover, bottom fluid cover, top fluid spacer (PDMS spacer I), bottom fluid spacer (PDMS spacer II), micro-aperture chip, and magnet. The assembling scheme is shown in Fig. 2a. The top fluid chamber was constructed by placing a layer of PDMS (thickness ~1.0 mm) on the micro-aperture chip, to serve as a spacer, and then mounting a 1 mm-thick glass slide on top of it. A laser cutter (Universal Laser System, Inc. Professional Series) was used to define the dimensions (30 mm by 3.8 mm) of the PDMS channel such that it enclosed the porous area (8560 μm by 2750 μm) of the micro-aperture chip. The silicon chip (thickness of 550 μm) with a porous area of 6 μm diameter micro-aperture arrays was fabricated following the procedures described in a previous publication.[53] The inlet and outlet for the upper chamber were formed by drilling holes through the glass slide using a diamond rotary bit. Tubing was sealed in place with epoxy. The bottom chamber was constructed with another PDMS layer (thickness ~0.2 mm) containing a channel (30 mm by 3.8 mm) fabricated with the laser cutter. The lower channel was sealed using a transparency sheet (3M PP2500, 0.1 mm thick). For the transparency sheet, the inlet and outlet holes were fabricated using the laser cutter. The bottom inlet and outlet tubing was connected to plastic elbow fittings and glued to the holes of the transparency sheet using epoxy. The assembled components were then mounted on an acrylic stand containing three rectangular openings. The middle opening was for inserting the magnet while the two openings on both sides provided space for the inlet and outlet tubing to emerge from the bottom chamber. All acrylic components were modified using the laser cutter. The top acrylic cover also contained a wide opening to enable quantification of cells directly on the chip surface using a fluorescence microscope.

Device modeling

COMSOL was used to model the influence of the micro-aperture chip surface on the magnetic bead trajectories. This was performed in order to quantify the number of beads that pass through the micro-apertures into the bottom chamber

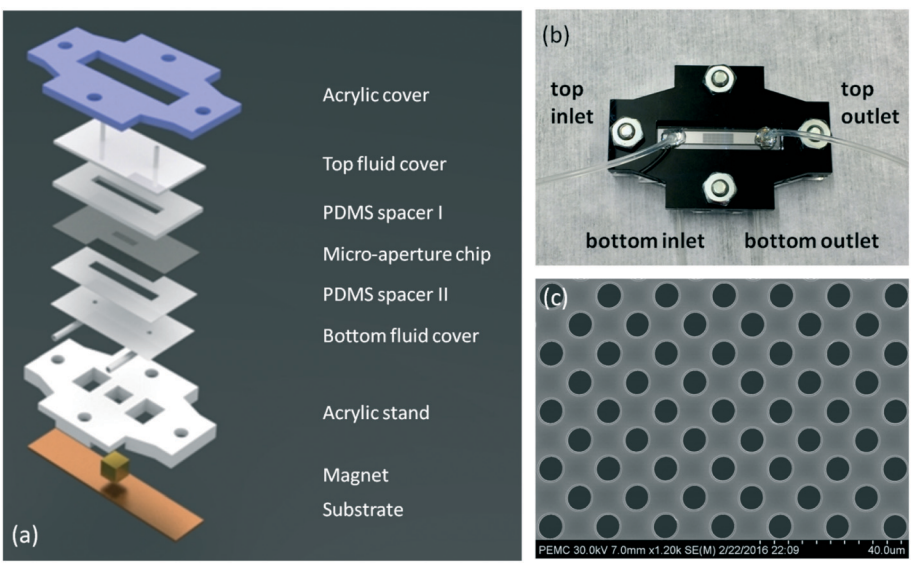

Fig. 2 Device assembly. (a) Exploded view of assembly scheme. (b) The assembled device. (c) SEM image of the micro-aperture chip containing an array of 6 μm diameter micro-apertures.

while flowing the suspension through the upper chamber of the device. All other simulation details, equations and conditions were similar to those in previous publications.[32,43] To simplify the modeling, only beads without cells were used for the simulations – the possibility of cells passing through holes *via* contortion or other shape modification was neglected.

Experimental setup

As described in "System and device assembly", two sets of inlets and outlets provided access to the top and bottom chambers. After priming the upper and lower chambers with PBS buffer, the bottom inlet and outlet were sealed. The top inlet was then connected to the sample source and the top outlet was connected to a peristaltic pump (New Era Pump Systems, NE-9000) which led to a waste container. This allowed the sample/bead mixture and buffer to flow only through the top chamber of the device. For sample circulation (using a closed-loop configuration), 300 μL of the test fluid was first injected followed by placing the pump outlet into the sample vial for the desired time. After circulation, the outlet tubing was placed back into the waste container as buffer was pumped through the device. In order to retrieve and collect the protein-bead complexes from the bottom chamber for downstream analysis after an experiment, the top inlet and outlet tubes were sealed, the bottom inlet tube was connected to the washing buffer (PBS) and the bottom outlet tube was connected to the pump. With the magnet removed, the beads could then be collected in a plastic tube at the outlet of the pump by flowing 1.5 mL of buffer.

Prior to running any experiments, PBS-T (PBS containing Tween 20) plus bovine serum albumin (BSA) was used to block the sample fluid-exposed surfaces of the device. The blocking solution consisted of 600 μL of 20× PBS-T (Thermo Fisher Scientific, USA), 400 μL of 30% BSA in PBS (Sigma, USA), and 11 mL of DI water. About 200 μL of this solution was injected into the upper chamber of the device and incubated for 3 hours at room temperature. Both the bottom and top chambers were then flushed with PBS.

Preparation of LNCaP cells and PSMA protein solution

LNCaP cells, purchased from American Type Culture Collection, were cultured in RPMI 1640 media (Gibco, USA) containing 10% fetal bovine serum (FBS, Gemini Bio Products). To harvest LNCaP cells, they were first released from a culture flask using a Trypsin–EDTA solution (Invitrogen) and then re-suspended in culture medium. The cell concentration was measured by taking 5 samples (each with a volume of 3 μL, ejected onto a microscope slide) and manually counting the cell number using a bright-field microscope to obtain the average. The cell suspensions were then subsequently spiked into 1 mL of medium (or diluted blood) to achieve the desired concentration.

Recombinant human PSMA/FOLH1 protein (PSMA) was purchased from R&D Systems and stored at −20 °C at a concentration of 0.5 mg mL^{-1} in PBS. PSMA was then diluted and spiked into medium or diluted human blood at desired concentrations.

Preparation of antibody-coupled magnetic beads

Biotinylated polyclonal anti-PSMA, anti-EpCAM, and anti-EGFR were all purchased from R&D Systems and stored at a concentration of 0.2 mg mL^{-1} in PBS. Prior to detection, the desired antibody was conjugated to micro-beads by incubating the antibody (10 μL) with streptavidin-coated 1 μm magnetic beads (20 μL, 10 mg mL^{-1}, Sigma Aldrich) in phosphate buffered saline (PBS, 70 μL) at room temperature for 60 min on an end-over-end rotator. An excess amount of antibody was used to ensure saturation of binding sites on the bead surface. Following incubation, the beads were washed 3 times with PBS using a magnetic stand (PerkinElmer, Germany) and then stored at 2 mg mL^{-1}.

Detection of LNCaP cells in the absence of free PSMA

The device was initially tested with multiple antibody-conjugated magnetic beads to determine which ligands and quantity of beads provided the highest capture efficiency of LNCaP cells. The new device enabled the doubling of the 1 μm bead amount able to be used in an assay, from 40 μg in the previous design to 80 μg.[43] This was due to the ability to clear the excess beads into the lower chamber. In these experiments, ~100 LNCaP cells were spiked into 1 mL of culture medium. The spiked samples were then incubated with either 40 μg (20 μL) or 80 μg (40 μL) of antibody beads at room temperature for 90 min using an end-over-end rotator. If a single antibody was used then 20 μL or 40 μL of only that bead suspension (2 mg mL^{-1}) was added. If two antibodies were used, then 20 μL of each antibody bead suspension was added. The sample was then circulated in the upper chamber of the device (with the bottom magnet in place) at a flow rate of 2 mL min^{-1} for 4 minutes followed by washing with 2 mL of PBS.

Following detection, any free beads which remained on the micro-aperture chip surface were gathered into the bottom chamber using a dual-magnet mode.[32] In the dual-magnet mode, a second, smaller magnet is placed on top of the entire device while keeping the bottom magnet in place. The top magnet is then moved back-and-forth, horizontally, in an oscillatory fashion. This perturbs the horizontal magnetic field for any beads on the chip surface, thus enabling their lateral movement that subsequently leads to beads falling through nearby micro-apertures, into the bottom chamber. Please see ESI† Fig. S1 for a comparison of the observed differences for the micro-chip surface (which enables the removal of protein-bound and free beads) in contrast to a chip which lacks the micro-aperture structure.

With only the bottom magnet in place, the captured cells were then directly fixed on the chip using a 4% paraformaldehyde (PFA) solution in PBS for 10 minutes at room temperature followed by fluorescent tagging for confirmation. To label the cells, monoclonal antibodies against PSMA

conjugated with PE (anti-PSMA-PE, Miltenyi Biotec, USA), anti-pan cytokeratin monoclonal antibodies conjugated to FITC (anti-CK-FITC, Miltenyi Biotec, USA), and 4′,6-diamidino-2-phenylindole (DAPI, Sigma-Aldrich, USA) were introduced into the top chamber all at once and incubated for 30 minutes at room temperature. Unbound labels were washed out with 3 mL of PBS. The micro-aperture chip was then inspected while still in the microfluidic device, using a fluorescence microscope (ECLIPSE 80i, Nikon) containing a fibre illuminator (C-HGFI, Nikon), to count the captured cells and determine the capture efficiency.

Detection of free PSMA in the absence of LNCaP cells

The detection of free PSMA (without LNCaP cells) was performed identically to that above for LNCaP cells without PSMA but with the following modification. For these experiments, only PSMA was spiked (0–12.5 nM, 0–1000 ng mL^{-1}) into 1 mL of culture media. Following detection, PSMA-bound beads and free beads were gathered in the bottom chamber as described above. Both magnets were then removed and 1.5 mL of PBS was introduced into the bottom chamber at a flow rate of 1.5 mL min^{-1} to wash out the beads, which were collected in a plastic tube.

These beads were then analysed by flowing the collected suspension into a chamber containing a glass slide with a magnet placed underneath for immuno-fluorescence analysis (see ESI† Fig. S1). Prior to analysing the samples and in order to prevent non-specific binding of antibodies, a PBS solution containing 0.05% Tween-20 and 1% BSA was introduced into the single-chamber device and allowed to incubate for 3 hours at room temperature. The device was then washed with 2 mL of PBS at a flow rate of 3 mL min^{-1}. Retrieved beads were injected and distributed along the chamber surface, as a result of the applied force from an external magnet. PSMA was subsequently stained with anti-PSMA-PE (1 : 20 dilution in PBS) and incubated under static conditions at room temperature for 30 minutes, followed by washing with 3 mL of PBS. Finally, the chamber was inspected using the fluorescence microscope for PSMA quantification.[43]

Dual detection of LNCaP cells and PSMA

The combined detection of LNCaP cells and PSMA from culture media was performed next. Here, a series of suspensions were prepared by spiking ~100 LNCaP cells and PSMA with various concentrations from 0 to 12.5 nM (0–1000 ng mL^{-1}) into 1 mL of culture medium. The samples were then incubated using the optimal antibody bead composition and analysed according to the two previous sections.

For detection in human blood, 1 mL of diluted blood (blood : PBS (1 : 3)) was prepared and used within 2 hours after being collected from healthy male volunteers under an approved IRB protocol. Blood samples were first drawn into BD vacutainer tubes containing sodium poly(anethol) sulfonate as the anti-coagulant prior to being diluted. For these experiments, LNCaP cells and/or free PSMA (in addition to the level of PSMA naturally present) were spiked into each sample. Four conditions were tested: (1) a blank without any added target protein or cells; (2) ~27 added LNCaP cells; (3) ~27 added LNCaP cells and 50 pM (4 ng mL^{-1}) of PSMA. (4) ~54 added LNCaP cells and 1.25 nM (100 ng mL^{-1}) of PSMA. It should be noted that the spiked PSMA concentrations provided are relative to the 1 mL diluted sample volume.

The diluted blood samples were then analysed similar to that for dual detection from media but with the following modifications. Prior to fixing the cells using PFA but after removing the beads from the bottom chamber, red blood cell (RBC) lysis buffer (G-Biosciences, U.S.A.) was introduced into the upper chamber and incubated for 5 min before rinsing with PBS. This was done in order to remove RBCs which were attracted to the magnet during the sample circulation step. Additionally, anti-CD45-PE was added to the dye cocktail for cell labelling in order to differentiate any white blood cells (WBCs) that might be present due to non-specific binding. Anti-PSMA-PE was removed from the dye cocktail so it would not overlap with the anti-CD45-PE signal due to their identical fluorescent labels (*i.e.* phycoerythrin (PE)).

Results and discussion

(1) Modeling the effect of the micro-aperture chip for magnetic bead capture

Previously, we used simulations to investigate how flow rate and the number of beads bound per cell would influence the trajectories of cell-bead complexes in our microfluidic device.[32,43] It was assumed in those simulations that the micro-aperture chip functioned as a solid surface (without pores) with respect to its ability to capture bead-bound cells. A finite element analysis software (COMSOL) was used to simulate the magnetic field, flow field, induced magnetic force and fluid drag force, as well as the gravitational and buoyant forces acting on cells and magnetic beads.[32] Here, we extend our characterization to account for the true 6 μm diameter micro-aperture array structure in order to determine the quantitative effect of the structure on the ability of protein-bead complexes and free beads to fall into the lower chamber of the device during sample flow.

For this work, the magnetization effect of particles on one another, the difference between a protein-bound bead and a free bead, and the effect of the micro-aperture chip's pore depth on a bead were all assumed to be negligible. It was also assumed that the beads were randomly distributed over the inlet cross-section as they were introduced into the chamber. Due to the low Reynolds number (R_e = 9.95) of the device, laminar flow was assumed for the simulation and the flow rate was set to 2 mL min^{-1} in accordance with previous experiments and simulations.[32,43]

Fig. 3 shows the simulation and trajectories of 100 superparamagnetic beads flowing inside the dual-chamber system. According to the results, a uniform flow field was quickly established following the introduction of beads into the upper chamber. Subsequently, 52% of the beads ended up in

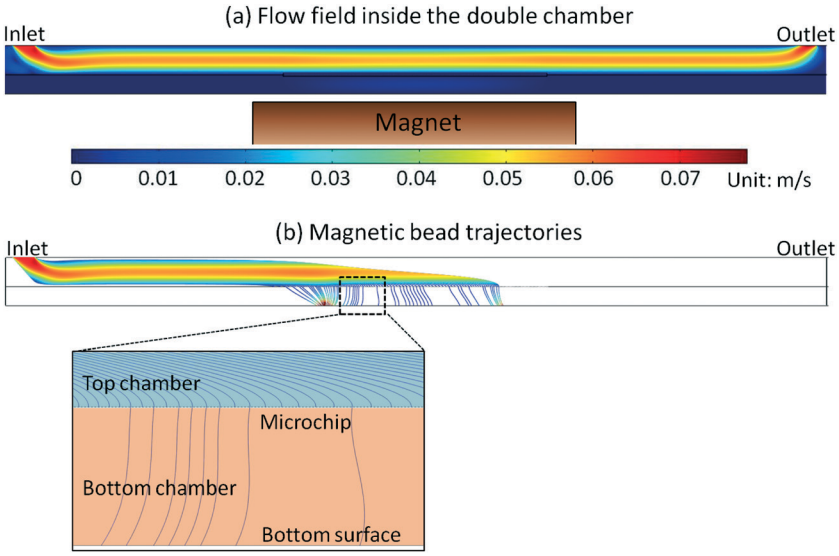

Fig. 3 Bead trajectory simulation results. (a) The flow field in the device with the inlet flow rate set to 2 mL min^{-1}. (b) Trajectories of magnetic beads in the dual-chamber system showing that 52% of the beads will fall through the micro-aperture holes during flow, indicating the need for a dual-magnet mode to aid in the removal of the remaining protein-bound beads and free beads that land on the chip surface.

the bottom chamber *via* the micro-aperture holes. This implied that, in order to aid in the visualization of cells in the upper chamber for actual experiments, a dual-magnet mode was going to be necessary. This allowed any remaining free beads on the micro-aperture chip surface to move laterally, find a hole, and fall into the bottom chamber.[32]

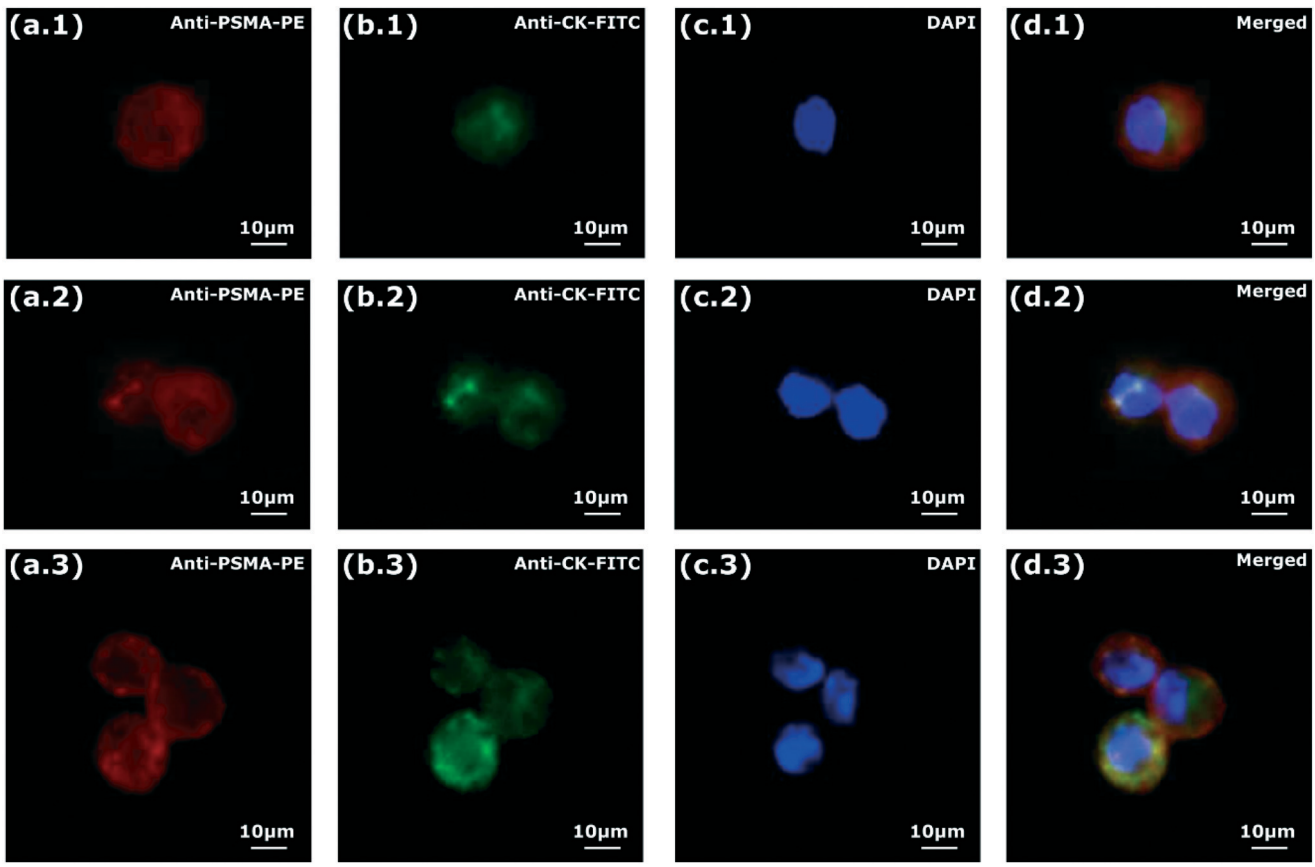

Fig. 4 Fluorescence images of LNCaP cells. Single cell (row 1), two cells (row 2), and three cells (row 3) were stained with anti-PSMA-PE (column a), anti-CK-FITC (column b), and DAPI (column c) to verify the identification of the LNCaP cells captured. Column d shows the merged image of columns (a) to (c) for each row.

(2) Cell detection in the absence of free PSMA

Beads conjugated with various antibodies were used to characterize the ability of the micro-aperture device for detecting rare cells without the presence of free target proteins. As LNCaP cells are known for expressing significant amounts of both PSMA and EpCAM surface markers, corresponding antibodies to these two antigens were initially investigated.[54] Using two quantities of magnetic beads (40 μg and 80 μg) for each target, antibody bead conjugates were prepared and tested in order to achieve the highest cell detection yield. Captured cells were verified based on a combination of factors including their size (8–30 μm), shape (close to circular), and fluorescence signals, wherein anti-PSMA-PE (+), anti-CK-FITC (+) and DAPI (+) cells were scored as a positive result (Fig. 4).

As shown in Fig. 5, both quantities of anti-PSMA-only beads led to the detection of ~50% of the spiked LNCaP cells. For EpCAM, while the average capture value for 80 μg of beads was higher than that for 40 μg (96% *versus* 88%), from a statistical perspective, the difference was not significant ($p > 0.05$). The higher capture for EpCAM compared to PSMA correlates with a higher level of expression for the former, which was confirmed using a fluorescence cell-labeling assay (see ESI† Fig. S2). These results indicated a level of expression for EpCAM that was about twice that of PSMA. As the goal of this work was to achieve dual detection of LNCaP cells and free PSMA protein, a 50% mixture of anti-EpCAM and anti-PSMA bead conjugates was then tested (40 μg of each). The data revealed that this combination was able to achieve the same high yield (~94%) as compared to using only anti-EpCAM beads. Thus, the presence of anti-PSMA did not interfere with the capture efficiency. It should be noted that since LNCaP cells express both surface antigens, it is possible that both antibody beads play a role in cell capture, especially due to the heterogeneous nature of cell populations.[55] For example, a small number of cells within the population may express more PSMA than EpCAM. However, anti-EpCAM, due to being significantly more expressed overall, is likely the major contributor to the high yield obtained for the bead mixture.

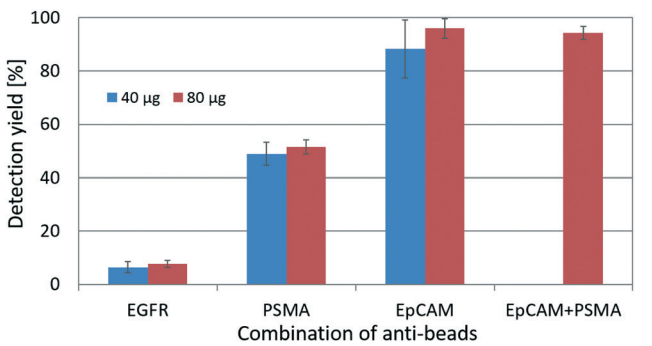

Fig. 5 LNCaP cell capture efficiency using different anti-bead combinations and bead quantities. Blue and red bars represent 40 μg and 80 μg, respectively, of total beads added to the cell-spiked media. In the case where a mixture of beads was used (EpCAM plus PSMA), 40 μg of each bead was added. Error bars represent one standard deviation based on three experiments.

In order to verify the specificity of PSMA and EpCAM ligands and to ensure that the antibody conjugated beads were not non-specifically capturing LNCaP cells, an antibody against one additional surface marker, epidermal growth factor receptor (EGFR), was tested as a negative control. Previous reports have indicated that LNCaP cells do not exhibit high levels of EGFR, which was also confirmed by our fluorescence staining experiments (see ESI† Fig. S2).[56] The results shown in Fig. 5 for anti-EGFR conjugated beads provide further evidence that LNCaP cells express very little EGFR as only a ~7% detection yield was achieved, for both amounts of beads tested.

We then validated the specificity of the PSMA and EpCAM antibody bead combination for our cellular targets using KB cells as an additional negative control. The KB cell line is commonly known for expressing high levels of folate receptor (FR) but only minor amounts of PSMA[57] and EpCAM (due to being a subline of HeLa cells).[58] Compared to LNCaP cells, KB cells were found to be captured at significantly lower levels using the anti-PSMA and anti-EpCAM bead combination (9% *versus* 95% LNCaP, Fig. S3†). This confirmed that our bead mixture is able to achieve a high capture efficiency of cells that over-express specific surface antigens. It should be mentioned that 9% (instead of 0%) of KB cells were captured because KB, due to being epithelial in nature, expresses some amount of EpCAM on the cell surface[59] which was also verified in a fluorescence staining experiment (see ESI† Fig. S2).

While a ~94% capture yield for LNCaP cells using a mixture of anti-PSMA and anti-EpCAM beads was achieved, there were still 6% which were not detected. Thus, we investigated whether these uncaptured cells passed through the micro-apertures into the bottom chamber. Following the detection of LNCaP cells on the micro-aperture chip surface, the bottom chamber was inspected using a bright-field microscope in order to observe the lower chamber surface (*i.e.* the transparent film) as well as the bottom of the micro-aperture holes – no cells were found. This indicates that the small number of uncaptured cells might have been lost due to the heterogeneous nature of the cell population, with several cells not expressing a sufficient amount of either PSMA or EpCAM antigen to enable a magnetic pull down to the micro-aperture surface. While expected to be minimal, it is also possible that some cells may have stuck to the walls of the sample tube or the tubing used in the fluidic system and hence may have been lost.

(3) Detection of free PSMA in the absence of LNCaP cells

Next, the ability of the micro-aperture device to detect free target proteins in the absence of cells was evaluated. Using the same procedures and conditions as for cell detection, different concentrations of free PSMA (0–12.5 nM, 0–1000 ng mL^{-1}) were spiked into 1 mL of culture medium. The sample

was then incubated with a 50% mixture of anti-PSMA and anti-EpCAM beads. Following the capture and elution of protein-bead complexes and free beads from the lower chamber of the micro-aperture device, the retrieved beads were subsequently injected into a single-chamber platform for fluorescence analysis. Fig. 6 shows the fluorescence and corresponding bright field images of the beads distributed on the single-chamber device glass surface for three different PSMA concentrations: 12.5 nM (1000 ng mL^{-1}), 1.25 nM (100 ng mL^{-1}), and 0 nM (0 ng mL^{-1}). Using these images with multiple PSMA spiked concentrations subsequently allowed the limit of detection (LOD) for the micro-aperture device to be determined.

In order to establish the numerical correlation between the input (PSMA concentration) and output (fluorescence) signals, we collected fluorescence images of the stained beads and the corresponding reversed bright-field image from the same observation window.[43] The fluorescence intensity was then normalized by the intensity of the reversed bright-field image, which was used as an estimation of the amount of beads in that observation window. The normalized intensity, termed the "*B*-ratio", thus represents the fluorescence signal per bead. The *B*-ratio was measured for eight different PSMA concentrations ranging from 0 to 12.5 nM (0–1000 ng mL^{-1}) as shown in Fig. 7. Performing a least squares Langmuir Isotherm fit to the experimental data revealed:

$$B_r = 0.222 + \frac{1.06}{1 + 2.97/C_p} \quad (1)$$

where B_r is the *B*-ratio; C_p is the PSMA concentration (nM); and 0.222 is the theoretical bias which is attributed to either non-specific binding between the fluorescent dye and antibody beads and/or the intrinsic fluorescence background of the magnetic beads. The theoretical bias agrees with our experimental *B*-ratio bias of 0.198, which was the observed response in the absence of PSMA. The

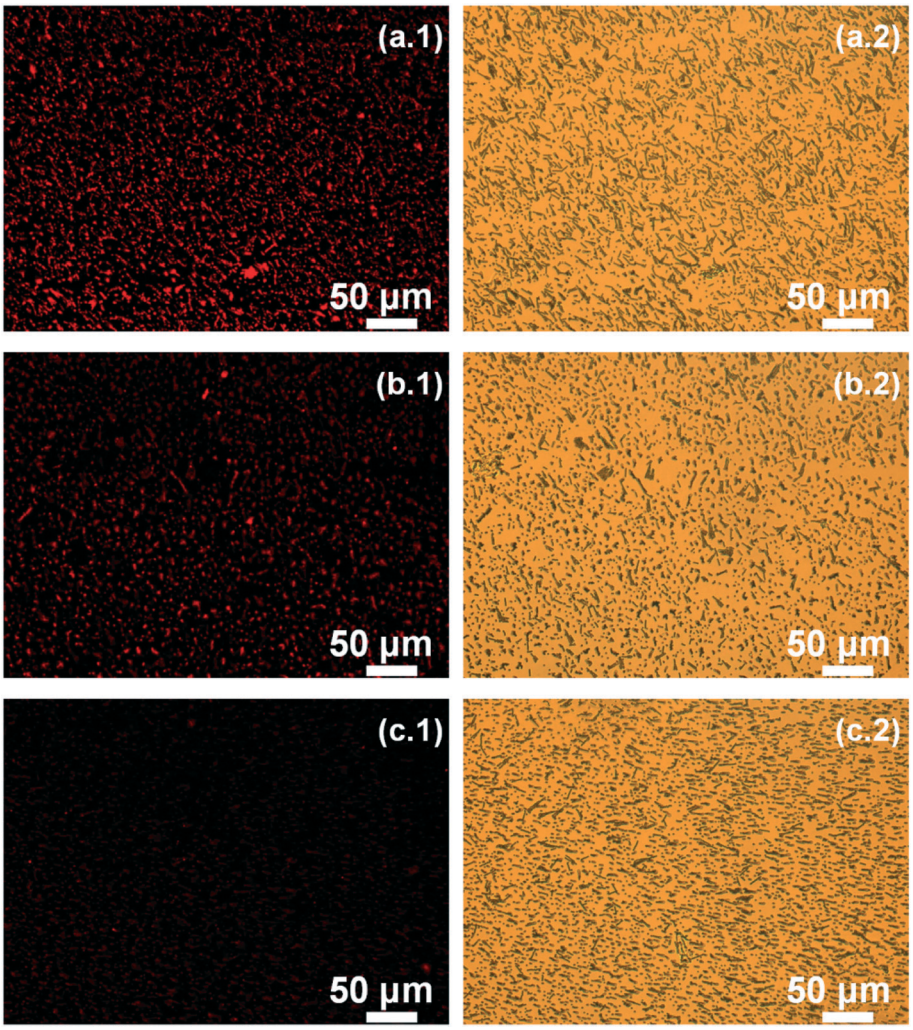

Fig. 6 Three pairs of fluorescence (column 1: left) and bright-field (column 2: right) images collected from cell media samples spiked with PSMA concentrations of 12.5 nM (1000 ng mL^{-1}) (row a), 1.25 nM (100 ng mL^{-1}) (row b), and 0 nM (0 ng mL^{-1}) (row c).

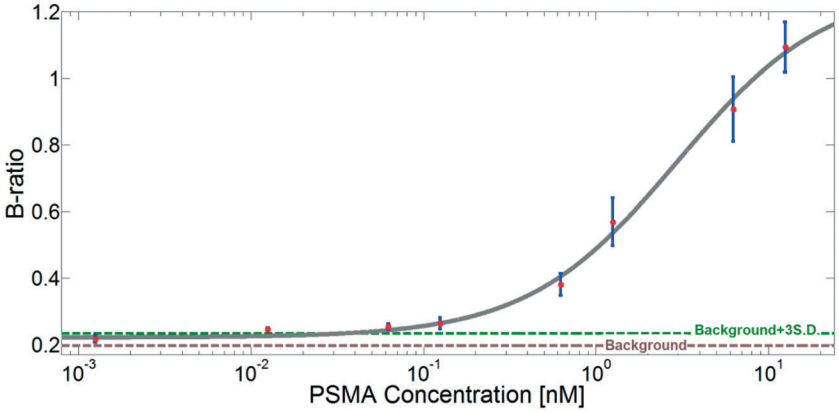

Fig. 7 The standard detection curve for free PSMA spiked into cell culture media using the anti-PSMA and anti-EpCAM bead mixture. The horizontal brown line represents the experimental background (*B*-ratio when PSMA = 0 nM) and the green line represents the background plus three standard deviations. The data reveals a limit of detection of 34 pM. Error bars indicate one standard deviation from three experiments for each concentration.

intersection of the fitted curve with the background-plus-three-standard-deviation line (see ESI† Fig. S4) corresponds to a PSMA spiked concentration of 34 pM (2.7 ng mL^{-1}), which we consider as the LOD for this assay using the new device. However, lower concentrations were still detectable (albeit not quantifiable based on our conservative definition of the LOD) using this assay. The effective dissociation constant (K_d) between anti-PSMA and PSMA was found to be approximately 3.0 nM, which is in reasonable agreement with previous reports.[60,61] While the simplicity of the overall method allowed a fluorescence assay to quantify free protein capture, the ability to easily retrieve the beads also enables the future use of other analytical techniques (*e.g.* flow cytometry, Luminex) to further expand the versatility and sensitivity of molecular concentration measurements.

As different combinations and amounts of antibody beads were analysed to maximize cell detection yield (section 2), we also investigated the contribution of anti-PSMA and anti-EpCAM for binding free PSMA. Here, various antibody bead combinations (80 μg of anti-EpCAM only, 80 μg of anti-PSMA only, and 40 μg of anti-EpCAM plus 40 μg of anti-PSMA) were tested using several concentrations of PSMA spiked into media (see ESI† Fig. S5). The results showed that anti-PSMA alone achieved the highest recovery, followed by the mixture of antibody beads. The use of only anti-EpCAM was found to have no significant effect on the ability to capture PSMA. While using only anti-PSMA beads would possibly allow for an improvement in the LOD for spiked PSMA, this would come at a loss in cell detection yield (Fig. 5). Thus, in order to achieve the highest yield for dual detection of cells and PSMA, a 50% bead mixture of anti-PSMA and anti-EpCAM beads was used for the remainder of this work. However, increasing the micro-aperture array area to accommodate an even larger number of beads, in a future device design, may lead to improved LODs for molecular targets while maintaining high cell capture efficiencies.

(4) Dual detection of LNCaP cells and free PSMA spiked into media

Next, the capability of the micro-aperture chip system for separating and detecting both LNCaP cells and free PSMA from a single sample fluid was tested. For these experiments, ~100 LNCaP cells and various concentrations (0–12.5 nM, 0–1000 ng mL^{-1}) of PSMA were spiked into culture medium (1 mL). The cell quantity and protein concentrations were chosen to be comparable to values reported for healthy human controls (PSMA only: 1–600 ng mL^{-1} (16 pM–7.5 nM)) and prostate cancer patients (PSMA: 350–950 ng mL^{-1} (4.38–11.9 nM) and CTCs: 0–400 per mL of whole blood).[62–66] Fig. 8 shows the measured PSMA concentration determined by eqn 1 (left *y*-axis) and the percentage of LNCaP cells captured (right *y*-axis) as a function of the PSMA concentration spiked into the media (*x*-axis). These results reveal several features. First, for PSMA spiked concentrations from 125 pM to 12.5 nM, the spiked concentrations (*x*-axis) and the measured

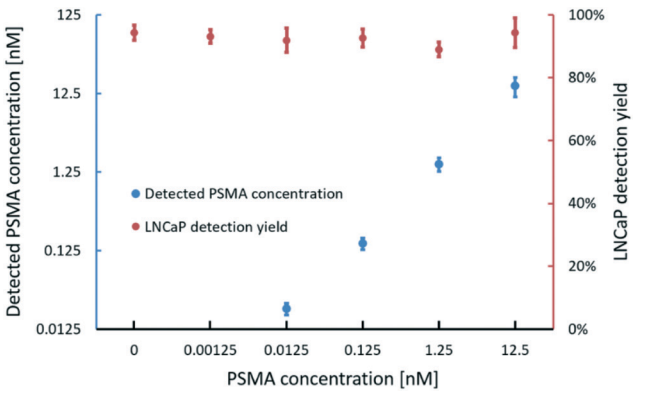

Fig. 8 The measured free PSMA concentration (left *y*-axis) based on eqn 1 and the detection yield of LNCaP cells (right *y*-axis) plotted against spiked PSMA concentration in culture medium (*x*-axis). Blue dots represent the detected PSMA concentration while red dots represent the LNCaP detection yield. Error bars indicate one standard deviation for three measurements.

concentrations (left *y*-axis) matched almost perfectly. However, the next lowest spiked condition (12.5 pM) was slightly above the measured value as determined from eqn 1. This is likely due to the low sensitivity in the detection curve at these concentrations and indicates that our conservative method to define the LOD (34 pM) as being three standard deviations from the baseline noise, is reasonable. For the lowest concentration analysed (1.25 pM) in this particular set of experiments, the measured PSMA value did not significantly differ from the background response (0 nM). Most importantly, for all samples tested, the micro-aperture device was able to detect LNCaP cells with a yield of ~93%.

The results from Fig. 8 confirm that the new device can detect multiple concentrations of PSMA while also capturing LNCaP cells. Furthermore, they also indicate that the cell detection yield is not significantly affected by the presence of free PSMA (p = 0.37 using a single factor ANOVA). One possible reason, as mentioned above, is that the anti-EpCAM beads play the dominant role in capturing a majority of the cells. The anti-PSMA beads thus play the major role in PSMA protein detection with a secondary benefit of helping anti-EpCAM in capturing more cells. As an additional check, the micro-aperture system was further characterized by simultaneously detecting a single concentration of PSMA (1.25 nM) in the presence of a variable number of LNCaP cells (0–80) using the anti-PSMA and anti-EpCAM bead mixture. Subsequent fluorescence analysis showed that the ability to capture free protein biomarkers was not significantly affected by the number of target cells present (see ESI† Fig. S6).

(5) Dual detection of LNCaP cells and free PSMA spiked into healthy human blood

In order to demonstrate the potential of the micro-aperture system for the simultaneous detection of cell and protein targets from clinical samples, LNCaP cells and PSMA were spiked into diluted healthy human blood which was used to simulate an actual prostate cancer patient. For these experiments, 250 μL of unprocessed whole blood was first diluted to 1 mL with PBS and then spiked with LNCaP cells and/or free PSMA, in addition to the level of PSMA naturally present. The sample was then incubated using the 50% mixture of anti-PSMA and anti-EpCAM beads, injected into the micro-aperture device, and analysed using similar procedures as above. The measured PSMA concentration was calculated using eqn 1. LNCaP cells were verified based on a combination of factors including their size (8–30 μm), shape (close to circular), and fluorescent signals, wherein anti-CK-FITC (+), anti-CD45-PE (−) and DAPI (+) cells were scored as a positive result. Anti-CD45-PE (+) and DAPI (+) cells were identified as white blood cells (WBCs). Example images are shown in Fig. 9.

For these experiments, four different conditions were tested (Fig. 10) using the diluted blood sample. The first condition (group 1) involved spiking ~54 LNCaP cells and 1.25 nM (100 ng mL^{-1}) of PSMA. Group 2 represents a sample containing ~27 spiked LNCaP cells and 50 pM (4 ng mL^{-1}) of spiked PSMA. Group 3 contained only ~27 LNCaP cells. Group 4 was used as a control containing no added target protein or added cells. It should be noted that the spiked PSMA concentrations provided are relative to the 1 mL diluted sample volume.

The results shown in Fig. 10 reveal several important features of the new device. First, for all conditions where LNCaP cells were added, a consistent detection efficiency of ~90% was obtained. This was true for both quantities of cells (*i.e.* 27 and 54 cells per 1 mL of diluted blood) as well as both concentrations of spiked PSMA (*i.e.* 50 pM and 1.25 nM) and is not significantly different from that achieved using culture media (~93%). The zero detected cells in the control samples (group 4) further indicates that the increased captured cell purity (*i.e.* the enhanced visualization of cells), due to the separation of protein-bound beads and free beads afforded by the micro-aperture chip, led to the elimination of any false-positive results. However, ~200 WBCs were also observed on the micro-aperture chip surface after each detection. This is likely the result of non-specific binding of WBCs *via* three mechanisms: (1) WBCs from blood adhering to the chip surface. (2) WBCs non-specifically binding to the magnetic beads in blood during incubation which are then attracted to the chip surface. (3) WBCs expressing small amounts of surface antigens and are thus captured by the anti-beads. To put this observation into perspective, using a conservative estimate, 250 μL of whole blood contains over ~1 million WBCs.[67] Thus, the device was able to remove more than 99.9% of endogenous leukocytes.

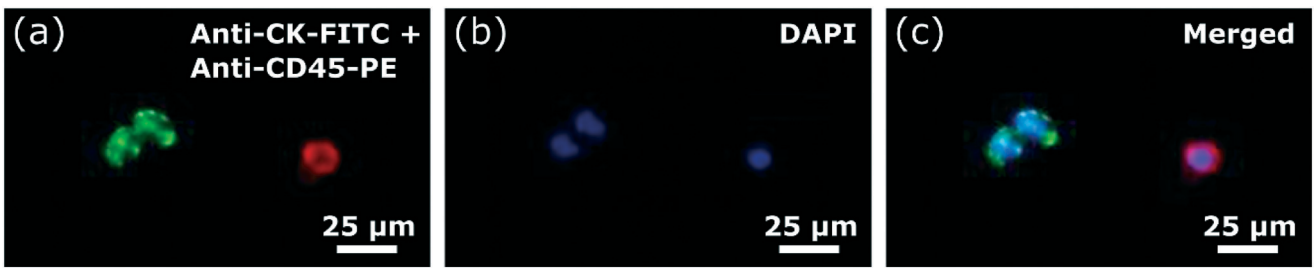

Fig. 9 Fluorescence images of captured cells. (a) LNCaP cells were first identified with anti-CK-FITC (green) and white blood cells were identified with anti-CD45-PE (red). (b) Cell nuclei were stained with DAPI. (c) Shows the merged image of panels (a) and (b). Images were artificially enhanced for clarity.

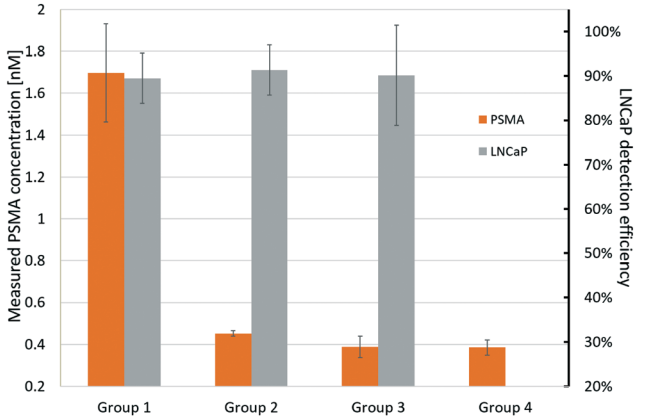

Fig. 10 The detection yield of LNCaP cells and the measured concentration of free PSMA obtained from diluted healthy human blood (1 : 3, blood : PBS). Grey columns represent the cell detection yield while the orange columns represent the measured PSMA concentration as determined from eqn 1. Zero cells were detected for group 4. The number of LNCaP cells spiked in groups 1, 2, 3, and 4 were approximately 57, 27, 27, and zero, respectively. The concentrations of PSMA spiked in groups 1, 2, 3, and 4 were 1.25 nM, 50 pM, 0 nM, and 0 nM, respectively. Error bars indicate one standard deviation for three measurements.

This level of purity and capture efficiency was achieved by integrating parallel fluid flow (relative to the surface of the micro-chip) of the blood sample, to enhance the removal of off-target normal blood cells from the micro-chip surface, with 6 μm apertures, which reduced the probability of targeted tumor cells (>8 μm)[68] from passing through the pores. Similarly, WBCs have typical diameters of 7–20 μm[67] and are thus also not expected to pass through the pores. In this work, spiked tumor cells captured from blood were only observed in the top chamber and nowhere else in the device. As RBCs can sustain a magnetic attraction and are deformable,[69,70] small amounts of these cells were initially observed in the device but they were readily removed using RBC lysis buffer and were not found to affect performance.

Now for PSMA, the measured concentration for group 3 and group 4 were nearly identical (both were approximately 0.39 nM (31 ng mL^{-1})) which revealed that the presence and capture of LNCaP cells did not interfere with free protein detection. The 0.39 nM measured PSMA concentration for the diluted sample is also consistent with previous studies using healthy human blood.[63,66] Spiking a PSMA concentration of 50 pM into the diluted sample (group 2) was found to be significantly different from the PSMA measured concentrations for groups 3 and 4 ($p < 0.05$). This appears to represent the lowest detectable concentration above background using this device coupled with the fluorescence quantification method utilized in this work. The lowest detectable concentration from diluted blood (50 pM above background) in Fig. 10 is larger than the lowest detectable concentration from culture media in Fig. 8 (12.5 pM). The difference in sensitivities is likely due to matrix effects (*e.g.* non-specific binding) which usually increases the background noise of the assay. However, this did not appear to affect cell capture yields. Lastly, the difference in the measured concentration of PSMA from group 1 compared to groups 3 and 4 (a difference of 1.31 nM) is similar to the theoretical difference in the spiked concentration (1.25 nM). This indicates that higher concentrations of target protein are still efficiently captured even when simultaneously detecting cells.

While the quantity of spiked LNCaP cells analysed in Fig. 10 falls into the expected numbers of CTCs observed in prostate cancer patients (0–400 CTCs per mL of whole blood), we also challenged the new device by performing dual detection at the lower end of this range. In order to detect (and accurately aliquot) a small number of target cells using conditions as similar as possible to that in Fig. 10, a larger volume of blood was necessary. Here, 1 mL of whole blood was diluted with PBS (to 4 mL), spiked with ~20 LNCaP cells and 50 pM of PSMA, and then incubated on an end-over-end rotator to homogenize the sample. The sample was then split into 4–1 mL tubes and each was individually analysed as above. A control sample without added PSMA or target cells was also tested. The results revealed that the number of LNCaP cells captured in consecutive tubes was 4, 6, 4, and 3 cells, which compared to zero cells detected in the control – the theoretically expected result was 5 cells per tube. Due to the stochastic distribution of a small number of cells in the 4 mL sample, the capture yield was calculated by summing the four individual tubes, revealing an 85% detection efficiency. For free PSMA, the concentration in the four tubes was uniformly distributed and was significantly different from the non-spiked control (a difference of ~80 pM, consistent with Fig. 10). Collectively, these results show the great potential of the micro-aperture device for dual detection of cell and protein targets from clinical samples.

Conclusions

We presented a dual-chamber, immuno-magnetic device capable of the simultaneous detection of cellular and molecular biomarkers of prostate cancer. The micro-aperture chip design provided affinity- and size-based separation of targets while enabling highly efficient capture of cells and proteins from a single sample fluid. The new platform yields cells in greater purity (*i.e.* the elimination of protein-bound or free magnetic beads), improves multi-ligand targeting by allowing for higher bead concentrations to be used in an assay, and enables further downstream analysis of captured analytes. Two types of prostate cancer biomarkers, free PSMA protein and LNCaP cells, were measured and used to characterize the device. The results demonstrated a 34 pM LOD of PSMA spiked into culture media. The detection yield of LNCaP cells was found to be independent of the PSMA concentration using a mixture of antibody beads against different cell markers, and to be consistently near ~93%. The dual measurement of PSMA and LNCaP cells was further demonstrated from diluted healthy human blood to mimic an actual cancer patient sample. For these experiments, the cell

detection yield was 85–90%, independent of the spiked PSMA concentration. The lowest detectable deviation in PSMA was found to be 50 pM for the diluted blood sample. The capability to simultaneously detect protein and cellular targets combined with the ability to extract desired rare cells for further investigation illustrates the potential of this device for high-throughput analysis of clinical samples. We plan to implement this platform in a forthcoming study using prostate cancer patients. In the future, we expect this system to be highly useful for a broad variety of applications including dual detection of CTCs and cell-free DNA.

Acknowledgements

We graciously acknowledge the generous gift from Thomas Hurvis that made this study possible.

References

1 R. L. Siegel, K. D. Miller and A. Jemal, *Ca-Cancer J. Clin.*, 2016, **66**, 7–30.
2 N. L. Henry and D. F. Hayes, *Mol. Oncol.*, 2012, **6**, 140–146.
3 C. L. Sawyers, *Nature*, 2008, **452**, 548–552.
4 N. Rifai, M. A. Gillette and S. A. Carr, *Nat. Biotechnol.*, 2006, **24**, 971–983.
5 M. Cristofanilli, D. F. Hayes, G. T. Budd, M. J. Ellis, A. Stopeck, J. M. Reuben, G. V. Doyle, J. Matera, W. J. Allard, M. C. Miller, H. A. Fritsche, G. N. Hortobagyi and L. W. Terstappen, *J. Clin. Oncol.*, 2005, **23**, 1420–1430.
6 D. C. Danila, G. Heller, G. A. Gignac, R. Gonzalez-Espinoza, A. Anand, E. Tanaka, H. Lilja, L. Schwartz, S. Larson, M. Fleisher and H. I. Scher, *Clin. Cancer Res.*, 2007, **13**, 7053–7058.
7 M. G. Krebs, R. L. Metcalf, L. Carter, G. Brady, F. H. Blackhall and C. Dive, *Nat. Rev. Clin. Oncol.*, 2014, **11**, 129–144.
8 E. Ozkumur, A. M. Shah, J. C. Ciciliano, B. L. Emmink, D. T. Miyamoto, E. Brachtel, M. Yu, P. I. Chen, B. Morgan, J. Trautwein, A. Kimura, S. Sengupta, S. L. Stott, N. M. Karabacak, T. A. Barber, J. R. Walsh, K. Smith, P. S. Spuhler, J. P. Sullivan, R. J. Lee, D. T. Ting, X. Luo, A. T. Shaw, A. Bardia, L. V. Sequist, D. N. Louis, S. Maheswaran, R. Kapur, D. A. Haber and M. Toner, *Sci. Transl. Med.*, 2013, **5**, 179ra47.
9 E. O. Weinberg, M. Shimpo, S. Hurwitz, S. Tominaga, J. L. Rouleau and R. T. Lee, *Circulation*, 2003, **107**, 721–726.
10 J. A. Ludwig and J. N. Weinstein, *Nat. Rev. Cancer*, 2005, **5**, 845–856.
11 S. M. Dhanasekaran, T. R. Barrette, D. Ghosh, R. Shah, S. Varambally, K. Kurachi, K. J. Pienta, M. A. Rubin and A. M. Chinnaiyan, *Nature*, 2001, **412**, 822–826.
12 P. S. Mitchell, R. K. Parkin, E. M. Kroh, B. R. Fritz, S. K. Wyman, E. L. Pogosova-Agadjanyan, A. Peterson, J. Noteboom, K. C. O'Briant, A. Allen, D. W. Lin, N. Urban, C. W. Drescher, B. S. Knudsen, D. L. Stirewalt, R. Gentleman, R. L. Vessella, P. S. Nelson, D. B. Martin and M. Tewari, *Proc. Natl. Acad. Sci. U. S. A.*, 2008, **105**, 10513–10518.
13 M. J. Duffy, N. O'Donovan, D. J. Brennan, W. M. Gallagher and B. M. Ryan, *Cancer Lett.*, 2007, **249**, 49–60.
14 P. Kanyong, S. Rawlinson and J. Davis, *J. Cancer*, 2016, **7**, 523–531.
15 V. A. Moyer and U. S. P. S. T. Force, *Ann. Intern. Med.*, 2012, **157**, 120–134.
16 T. W. Friedlander and L. Fong, *J. Clin. Oncol.*, 2014, **32**, 1104–1106.
17 B. Hu, H. Rochefort and A. Goldkorn, *Cancers*, 2013, **5**, 1676–1690.
18 P. Paterlini-Brechot and N. L. Benali, *Cancer Lett.*, 2007, **253**, 180–204.
19 J. S. de Bono, H. I. Scher, R. B. Montgomery, C. Parker, M. C. Miller, H. Tissing, G. V. Doyle, L. W. Terstappen, K. J. Pienta and D. Raghavan, *Clin. Cancer Res.*, 2008, **14**, 6302–6309.
20 E. Diamond, G. Y. Lee, N. H. Akhtar, B. J. Kirby, P. Giannakakou, S. T. Tagawa and D. M. Nanus, *Front. Oncol.*, 2012, **2**, 131.
21 A. J. Armstrong, M. S. Marengo, S. Oltean, G. Kemeny, R. L. Bitting, J. D. Turnbull, C. I. Herold, P. K. Marcom, D. J. George and M. A. Garcia-Blanco, *Mol. Cancer Res.*, 2011, **9**, 997–1007.
22 O. B. Goodman, Jr., J. T. Symanowski, A. Loudyi, L. M. Fink, D. C. Ward and N. J. Vogelzang, *Clin. Genitourin. Cancer*, 2011, **9**, 31–38.
23 O. B. Goodman, Jr., L. M. Fink, J. T. Symanowski, B. Wong, B. Grobaski, D. Pomerantz, Y. Ma, D. C. Ward and N. J. Vogelzang, *Cancer Epidemiol., Biomarkers Prev.*, 2009, **18**, 1904–1913.
24 K. Chang, Y. Y. Kong, B. Dai, D. W. Ye, Y. Y. Qu, Y. Wang, Z. W. Jia and G. X. Li, *Oncotarget*, 2015, **6**, 41825–41836.
25 A. de Gramont, S. Watson, L. M. Ellis, J. Rodon, J. Tabernero, A. de Gramont and S. R. Hamilton, *Nat. Rev. Clin. Oncol.*, 2015, **12**, 197–212.
26 R. Mayeux, *Neurotherapeutics*, 2004, **1**, 182–188.
27 E. Drucker and K. Krapfenbauer, *EPMA J.*, 2013, **4**, 7.
28 R. Smolders, H. M. Koch, R. K. Moos, J. Cocker, K. Jones, N. Warren, L. Levy, R. Bevan, S. M. Hays and L. L. Aylward, *Toxicol. Lett.*, 2014, **231**, 249–260.
29 E. Ingelsson, M. J. Pencina, G. H. Tofler, E. J. Benjamin, K. J. Lanier, P. F. Jacques, C. S. Fox, J. B. Meigs, D. Levy, M. G. Larson, J. Selhub, R. B. D'Agostino, Sr., T. J. Wang and R. S. Vasan, *Circulation*, 2007, **116**, 984–992.
30 A. Pikula, A. S. Beiser, C. DeCarli, J. J. Himali, S. Debette, R. Au, J. Selhub, G. H. Toffler, T. J. Wang, J. B. Meigs, M. Kelly-Hayes, C. S. Kase, P. A. Wolf, R. S. Vasan and S. Seshadri, *Circulation*, 2012, **125**, 2100–2107.
31 T. J. Wang, P. Gona, M. G. Larson, D. Levy, E. J. Benjamin, G. H. Tofler, P. F. Jacques, J. B. Meigs, N. Rifai, J. Selhub, S. J. Robins, C. Newton-Cheh and R. S. Vasan, *Hypertension*, 2007, **49**, 432–438.
32 C. L. Chang, W. Huang, S. I. Jalal, B. D. Chan, A. Mahmood, S. Shahda, B. H. O'Neil, D. E. Matei and C. A. Savran, *Lab Chip*, 2015, **15**, 1677–1688.

33 S. H. Cho, J. M. Godin, C. H. Chen, W. Qiao, H. Lee and Y. H. Lo, *Biomicrofluidics*, 2010, **4**, 043001.
34 K. Hoshino, Y. Y. Huang, N. Lane, M. Huebschman, J. W. Uhr, E. P. Frenkel and X. J. Zhang, *Lab Chip*, 2011, **11**, 3449–3457.
35 X. Y. Hu, P. H. Bessette, J. R. Qian, C. D. Meinhart, P. S. Daugherty and H. T. Soh, *Proc. Natl. Acad. Sci. U. S. A.*, 2005, **102**, 15757–15761.
36 S. I. Stoeva, J. S. Lee, J. E. Smith, S. T. Rosen and C. A. Mirkin, *J. Am. Chem. Soc.*, 2006, **128**, 8378–8379.
37 M. S. Wilson, *Anal. Chem.*, 2005, **77**, 1496–1502.
38 G. Zheng, F. Patolsky, Y. Cui, W. U. Wang and C. M. Lieber, *Nat. Biotechnol.*, 2005, **23**, 1294–1301.
39 J. M. Hou, A. Greystoke, L. Lancashire, J. Cummings, T. Ward, R. Board, E. Amir, S. Hughes, M. Krebs, A. Hughes, M. Ranson, P. Lorigan, C. Dive and F. H. Blackhall, *Am. J. Pathol.*, 2009, **175**, 808–816.
40 J. A. Bastarache, T. Koyama, N. E. Wickersham, D. B. Mitchell, R. L. Mernaugh, L. B. Ware and J. Immunol, *Methods*, 2011, **367**, 33–39.
41 P. O. Krutzik, M. R. Clutter, A. Trejo and G. P. Nolan, in *Current Protocols in Cytometry*, John Wiley & Sons, Inc., 2001.
42 P. Lea, E. Keystone, S. Mudumba A. Kahama, S. F. Ding, J. Hansen, A. A. Azad, S. H. Wang and D. Weber, *Clin. Rev. Allergy Immunol.*, 2011, **41**, 20–35.
43 W. Huang, C. L. Chang, B. D. Chan, S. I. Jalal, D. E. Matei, P. S. Low and C. A. Savran, *Anal. Chem.*, 2015, **87**, 10205–10212.
44 A. Ghosh and W. D. Heston, *J. Cell. Biochem.*, 2004, **91**, 528–539.
45 S. S. Chang, *Rev. Urol.*, 2004, **6**, S13–18.
46 G. Galletti, L. Portella, S. T. Tagawa, B. J. Kirby, P. Giannakakou and D. M. Nanus, *Mol. Diagn. Ther.*, 2014, **18**, 389–402.
47 R. Riesenberg, A. Buchner, H. Pohla and H. Lindhofer, *J. Histochem. Cytochem.*, 2001, **49**, 911–917.
48 R. E. Sobel and M. D. Sadar, *J. Urol.*, 2005, **173**, 342–359.
49 V. Yao and D. J. Bacich, *Prostate*, 2006, **66**, 867–875.
50 P. K. Grover, A. G. Cummins, T. J. Price, I. C. Roberts-Thomson and J. E. Hardingham, *Ann. Oncol.*, 2014, **25**, 1506–1516.
51 C. O. Madu and Y. Lu, *J. Cancer*, 2010, **1**, 150–177.
52 Y. H. Park, H. W. Shin, A. R. Jung, O. S. Kwon, Y.-J. Choi, J. Park and J. Y. Lee, *Sci. Rep.*, 2016, **6**, 30386.
53 C. L. Chang, S. I. Jalal, W. Huang, A. Mahmood, D. E. Matei and C. A. Savran, *IEEE Sens. J.*, 2014, **14**, 3008–3013.
54 B. J. Kirby, M. Jodari, M. S. Loftus, G. Gakhar, E. D. Pratt, C. Chanel-Vos, J. P. Gleghorn, S. M. Santana, H. Liu, J. P. Smith, V. N. Navarro, S. T. Tagawa, N. H. Bander, D. M. Nanus and P. Giannakakou, *PLoS One*, 2012, **7**, e35976.
55 C. Ma, R. Fan, H. Ahmad, Q. H. Shi, B. Comin-Anduix, T. Chodon, R. C. Koya, C. C. Liu, G. A. Kwong, C. G. Radu, A. Ribas and J. R. Heath, *Nat. Med.*, 2011, **17**, 738–743.
56 E. R. Sherwood, J. L. Van Dongen, C. G. Wood, S. Liao, J. M. Kozlowski and C. Lee, *Br. J. Cancer*, 1998, **77**, 855–861.
57 S. A. Kularatne, K. Wang, H. K. Santhapuram and P. S. Low, *Mol. Pharmaceutics*, 2009, **6**, 780–789.
58 B. R. Cheng, H. B. Song, S. Y. Wang, C. X. Zhang, B. B. Wu, Y. Y. Chen, F. F. Chen and B. Xiong, *Transl. Oncol.*, 2014, **7**, 720–725.
59 S. Gadadhar and A. A. Karande, *PLoS One*, 2013, **8**, e58304.
60 P. M. Smith-Jones, S. Vallabahajosula, S. J. Goldsmith, V. Navarro, C. J. Hunter, D. Bastidas and N. H. Bander, *Cancer Res.*, 2000, **60**, 5237–5243.
61 Y. Sugimoto, M. Hirota, K. Yoshikawa, M. Sumitomo, K. Nakamura, R. Ueda, R. Niwa, T. Suzawa, M. Yamasaki, K. Shitara, T. Kato and K. Nakamura, *Anticancer Res.*, 2014, **34**, 89–97.
62 D. C. Danila, M. Fleisher and H. I. Scher, *Clin. Cancer Res.*, 2011, **17**, 3903–3912.
63 T. Knedlik, V. Navratil, V. Vik, D. Pacik, P. Sacha and J. Konvalinka, *Prostate*, 2014, **74**, 768–780.
64 S. Nagrath, L. V. Sequist, S. Maheswaran, D. W. Bell, D. Irimia, L. Ulkus, M. R. Smith, E. L. Kwak, S. Digumarthy, A. Muzikansky, P. Ryan, U. J. Balis, R. G. Tompkins, D. A. Haber and M. Toner, *Nature*, 2007, **450**, 1235–1239.
65 S. L. Stott, C. H. Hsu, D. I. Tsukrov, M. Yu, D. T. Miyamoto, B. A. Waltman, S. M. Rothenberg, A. M. Shah, M. E. Smas, G. K. Korir, F. P. Floyd, A. J. Gilman, J. B. Lord, D. Winokur, S. Springer, D. Irimia, S. Nagrath, L. V. Sequist, R. J. Lee, K. J. Isselbacher, S. Maheswaran, D. A. Haber and M. Toner, *Proc. Natl. Acad. Sci. U. S. A.*, 2010, **107**, 18392–18397.
66 Z. Xiao, B. L. Adam, L. H. Cazares, M. A. Clements, J. W. Davis, P. F. Schellhammer, E. A. Dalmasso and G. L. Wright, Jr., *Cancer Res.*, 2001, **61**, 6029–6033.
67 A. C. Ritchi, in *Biomaterials Science*, ed. A. S. Hoffman, F. J. Schoen and J. E. Lemons, Academic Press, 2013, pp. 827–841.
68 S. Park, R. R. Ang, S. P. Duffy, J. Bazov, K. N. Chi, P. C. Black and H. S. Ma, *PLoS One*, 2014, **9**, e85264.
69 Y. Z. Yoon, H. Hong, A. Brown, D. C. Kim, D. J. Kang, V. L. Lew and P. Cicuta, *Biophys. J.*, 2009, **97**, 1606–1615.
70 M. Zborowski, G. R. Ostera, L. R. Moore, S. Milliron, J. J. Chalmers and A. N. Schechter, *Biophys. J.*, 2003, **84**, 2638–2645.

